Structure of the Cretaceous Kerguelen Volcanic Province (southern Indian Ocean) from wide-angle seismic data.

Philippe Charvis[a,*], Stéphane Operto[b]

[a]*ORSTOM, UMR Géosciences Azur, BP 48, 06235, Villefranche-sur-mer, Cedex, France*
[b]*UMR Géosciences Azur du CNRS, BP 48, 06235, Villefranche-sur-mer, Cedex, France*

Abstract

Travel time inversion and amplitude modelling of OBS wide-angle seismic data recorded in the Enderby Basin, west of the Kerguelen Plateau, show a 10 to 13 km thick crust characteristic of oceanic crust emplaced near a hotspot (velocity reaches 7.4 km s^{-1} at the bottom of the crust). From this study we infer that the eastern border of the Enderby Basin is part of the Cretaceous Kerguelen Volcanic Province, and that it results of the influence of the Kerguelen hotspot on the spreading axis. Synthetic seismogram modelling confirms that the northern Kerguelen Plateau is probably emplaced over the Kerguelen hotspot in an Iceland-type setting. © 1999 Elsevier Science Ltd. All rights reserved.

1. Introduction

The Kerguelen Plateau (KP) is a 2300 km-long, 200 to 600 km-wide submarine plateau stretching NNW–SSE from 46°S to 64°S in the southern Indian Ocean (Figure 1). It is surrounded by the Crozet Basin to the North, the Enderby Basin to the West, the Australian–Antarctic Basin to the East and the Princess Elisabeth trough to the South. The KP is usually divided into 3 major morphological units (Houtz et al., 1977; Coffin et al., 1986).

Between 46°S and 54°S, the northern KP is ~600 m below sea level (bsl) on average and emerges in the Kerguelen Archipelago, Heard and McDonald Islands. Several buried volcanic peaks aligned along the western border of the northern KP between Heard and Kerguelen Isles (Coffin et al., 1986; Munschy and Schlich, 1987) appear as heights on the free-air gravity map (Fig. 1). Although the basement of the northern KP was never sampled, an age of 100–120 Ma was extrapolated from biostratigraphic dating of the overlying sedimentary cover (Wicquart and Fröhlich, 1986).

---

* Corresponding author. Tel.: +(33) 4 93 76 38 83; fax: (33) 4 93 76 37 68; e-mail: charvis@obs-vlfr.fr
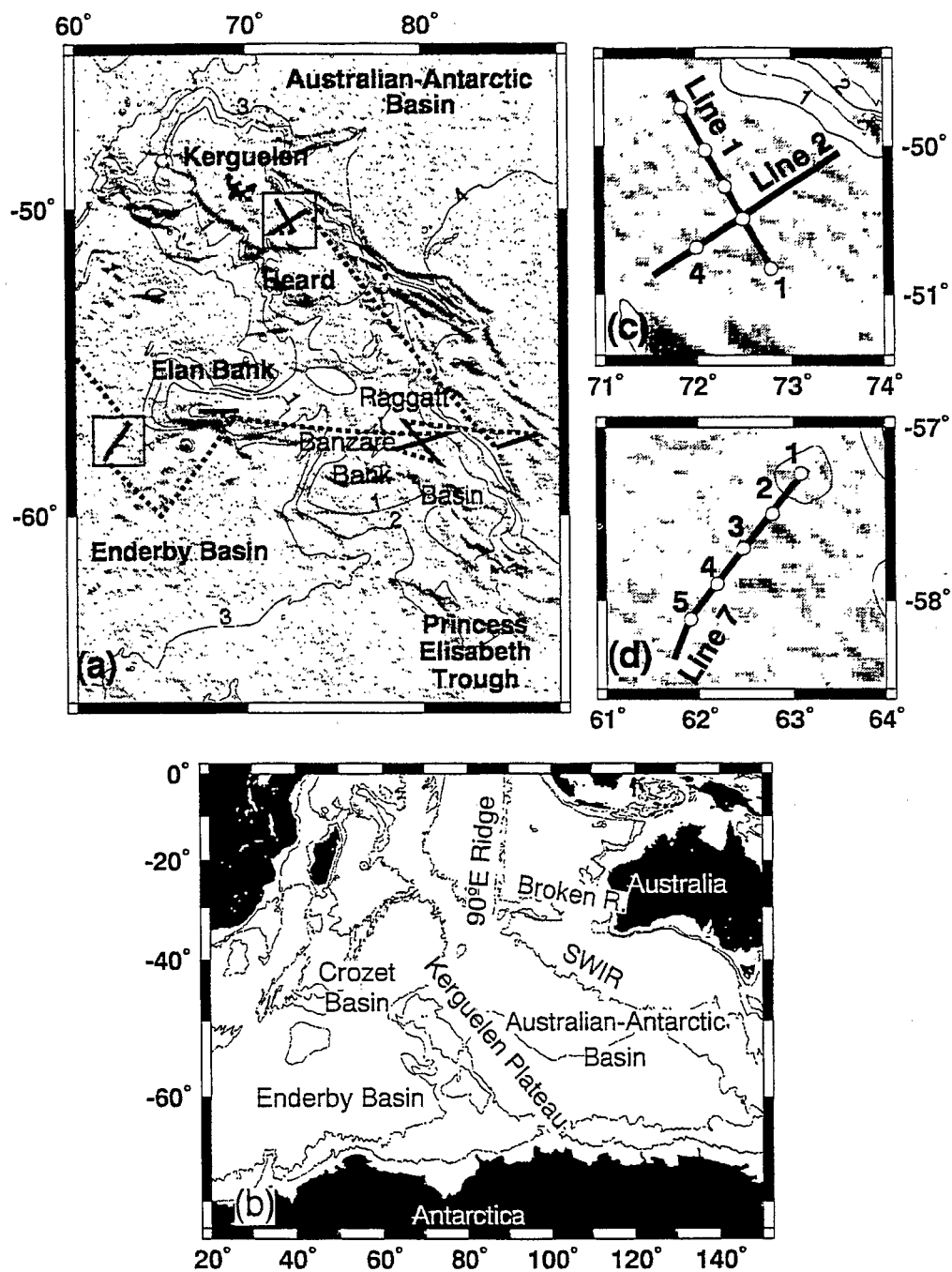
Fig. 1. (a) Bathymetric map of the Kerguelen Plateau after Schlich et al. (1987) modified using KeOBS bathymetric data. Contour interval is 1 km. Shading corresponds to the satellite-derived free-air gravity anomaly (Sandwell and Smith, 1994). Tracks of the KeOBS experiment are indicated (dashed lines) and location of refraction profiles, labelled from 1 to 7, are marked by thick lines. (b) Bathymetric map of the southern Indian Ocean from ETOPO-5 data (National Geophysical Data Center, 1988). Only bathymetric contours 2000 and 4000 m are drawn. (c) Detailed OBS positions for lines 1 and 2 (circles). (d) Detailed OBS positions (circles) for line 7.

Between 54° and 64°S, the southern KP lies 1500 m bsl. A large sedimentary basin, the Raggatt Basin, lies in the eastern part whereas the western part is occupied by a large volcanic feature, the Banzare Bank. The basement of the southern KP, sampled during ODP Leg 119 and 120 (Schlich et al., 1989), consists of tholeiitic basalts with radiometric ages ranging from 80 to 114 Ma (Whitechurch et al., 1992; Pringle et al., 1994).

At 56°S, the northern and the southern domains of the KP are separated by a transition zone of complex bathymetry. Immediately west of this transition zone, lies the Elan Bank, a major 600 km-long, E–W trending ridge (Fig. 1). Very little is known about this feature whose origin is not necessarily related to those of the Cretaceous KP (Coffin et al., 1986).

The western border of the southern KP is characterised by a gentle slope dipping toward the deep Enderby oceanic Basin. Eastward, the KP is bounded, south of 48°S, by a major fault scarp related to the rifting between the KP and Broken Ridge that culminated in break-up at 43 Ma (anomaly C18, Royer and Sandwell, 1989; Royer and Coffin, 1992). Before 43 My, the KP and Broken Ridge formed a single feature named, in this paper, the Cretaceous Kerguelen Plateau.

Whereas the KP, south of 50°S, clearly results from Cretaceous magmatism, the Kerguelen Archipelago and the northernmost end of the KP (north of 50°S) were emplaced after the break-up between Broken Ridge and the KP (i.e., 43 Ma, Giret, 1983; Munschy et al., 1992; Charvis et al., 1995). However, the submarine basement has never been sampled.

The Enderby Basin is a large oceanic basin, more than 4000 m deep, located between the KP and the Antarctic continental margin to the South. The age of the Enderby Basin is unknown due to the lack of datable magnetic anomalies but it is likely to be contemporaneous with the Cretaceous KP (Royer and Coffin, 1992).

Seven refraction lines were shot at sea in early 1991 on the KP and in adjacent oceanic basins during the MD66/KeOBS cruise (KeOBS stands for Kerguelen-OBS) on M.V. 'Marion Dufresne' (Charvis et al., 1995; Operto, 1995). In this paper, we present the deep structure of the Enderby Basin inferred from travel times inversion and synthetic seismogram modelling of wide-angle seismic line 7 (Fig. 1). We also describe a refined seismic model of the upper crust inferred from synthetic seismogram modelling along seismic lines 1 and 2 shot in the northern KP (Fig. 1).

The seismic source consisted of an untuned array of 8 16-litre air guns fired every 100 s (180 m). The receivers consisted of 5 3-component digital OBSs (Nakamura et al., 1987) evenly spaced along the 125 km long shooting line. A detailed description of data acquisition is provided in Operto and Charvis (1996).

Data were processed first using a zero phase Butterworth band-pass filter between 5 and 15 Hz (Figs 2 and 3). Predictive spectral deconvolution was applied afterwards to ease picking of secondary arrivals (PbP and PmP reflections, Fig. 3).

2. The Enderby Basin

2.1. Description of the data

The central OBS 3 record section is the most representative (Fig. 2). All the phases are distinctly observed with a very high signal-to-noise ratio (Fig. 3). Furthermore, the symmetry between the south-western and north-eastern part of the section suggests no large-scale lateral variation near
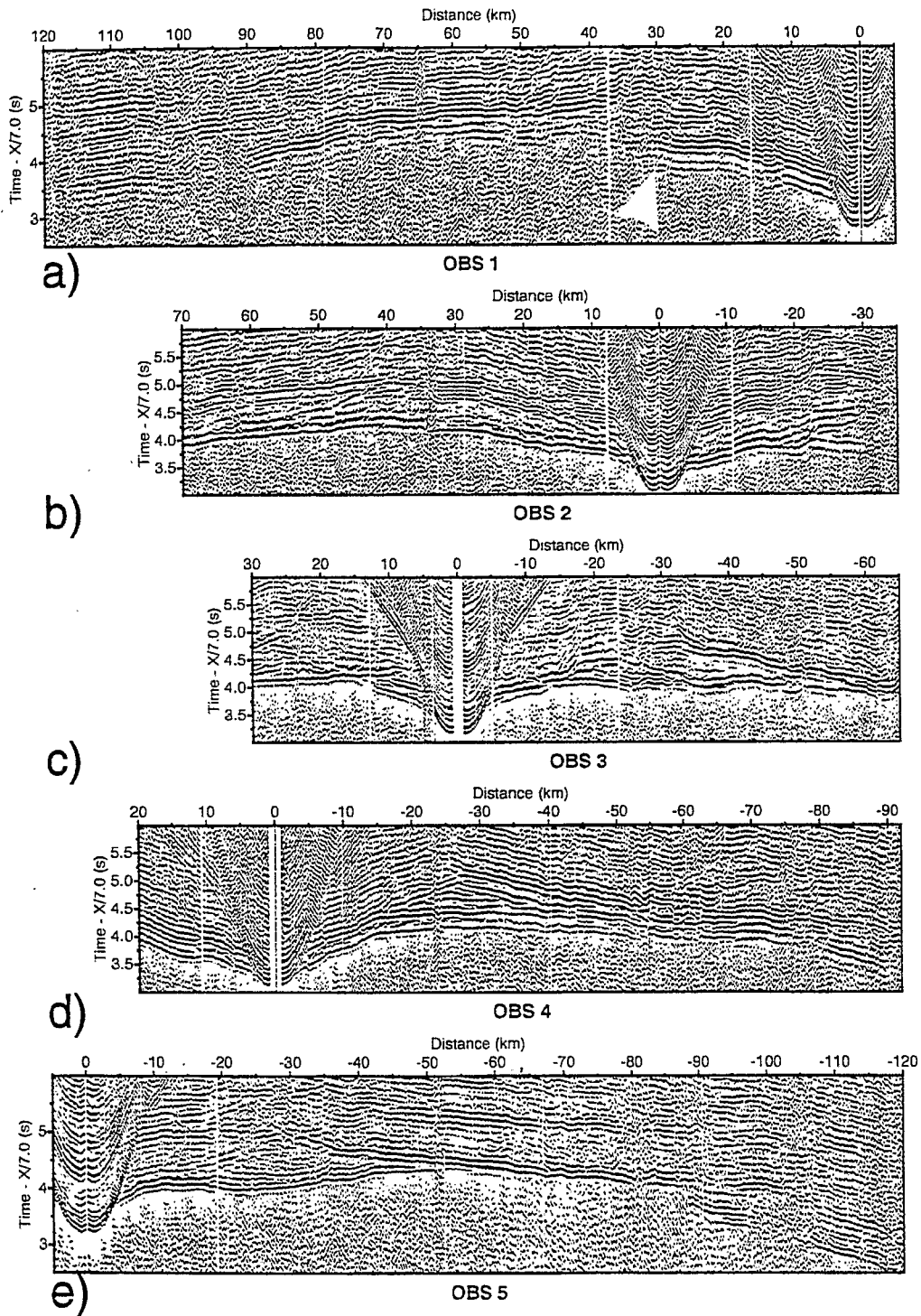
Fig. 2. Record sections along line 7. Data were processed using a predictive deconvolution (whitening), a 5–15 Hz zero phase Butterworth filter and an automatic gain control. Reducing velocity is 7.0 km s^{-1}. (a) OBS 1, the white arrow indicates the interruption of arrival P2 (see text for details). (b) OBS 2. (c) OBS 3. (d) OBS 4. (e) OBS 5.
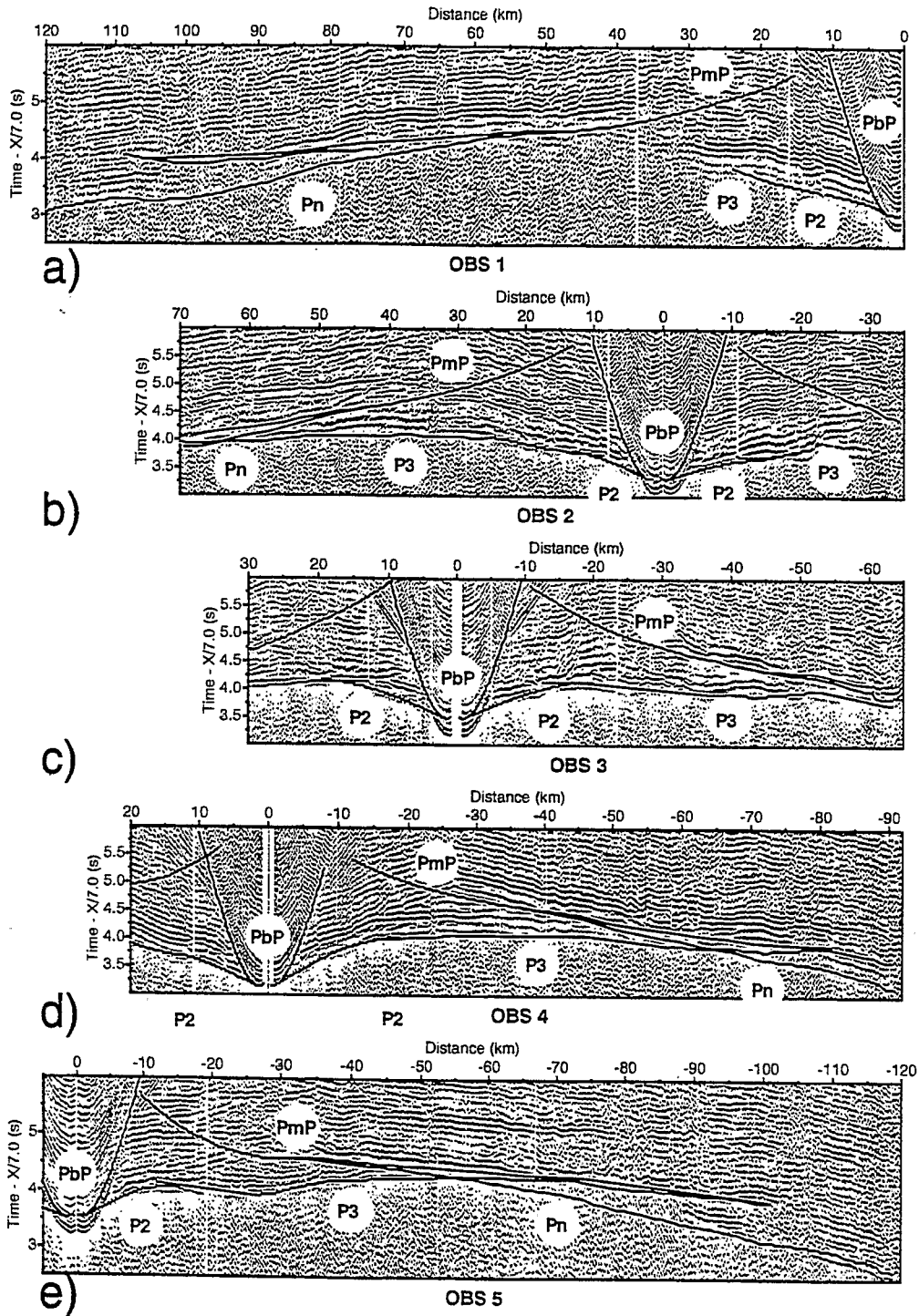
Fig. 3. (a) Record section from OBS 1 with superimposed travel time curves predicted by the model of Fig. 4. (b) same for OBS 2. (c) same for OBS 3. (d) same for OBS 4. (e) same for OBS 5. PbP: reflection from top of oceanic basement; P2: refraction in the upper crust. P3: refraction in the lower crust. PmP: wide-angle reflection from Moho. Pn: refraction in the upper mantle.

OBS 3. No refracted wave in the sedimentary cover is observed on any record section. Nevertheless, a thin sedimentary cover can be inferred from the delay time at zero-offset between the direct water wave and the reflection from the top of the oceanic crust (labelled PbP, Fig. 3). In the absence of further information, a seismic velocity of $1.6 \, km \, s^{-1}$, in the sedimentary layer, was chosen for the P-wave. This low velocity can account for the high amplitude of reflection from the top of the oceanic crust and for the apparent lack of refraction in the sedimentary cover (high amplitude water wave arrivals possibly hide the refraction in the sedimentary layer). Phases P2 and P3 propagate, respectively, as refracted waves in layer 2 and 3 (as defined for standard oceanic crust). A triplication related to velocity and/or gradient discontinuity between the bottom of layer 2 and the top of layer 3 underlined the P2–P3 cusp on OBS record section 3. The P2–P3 cusp is not identified clearly on other OBS record sections due to the roughness of the layer 2– layer 3 interface (Fig. 2). Moreover, the structural complexities of the upper crust are also displayed on OBS record section 1 by the sudden disruption of arrival P3 that is relayed, 0.4 s later, by an arrival bearing the same velocity [Fig. 2(a) and Fig. 3(a)] possibly related to tectonic features in the upper crust. The PmP wave, reflected from the Moho, appears clearly on all the record sections and the Pn, refracted in the upper mantle is visible on OBS record sections 1 and 5 but also probably exists on record section 4 (Figures 2–3).

2.2. Interpretation

2.2.1. Travel time inversion

A first velocity model was developed using a 2-D iterative damped least-squares inversion of travel times (Zelt and Smith, 1992). Because of the roughness of the crustal interfaces (mainly sediment-layer 2, and layer 2–layer 3 interfaces), just one iteration was done to derive the gross velocity structure using a coarse parameterisation for the model. Subsequently, short-wavelength variations of the interfaces were modelled by a trial-and-error approach using a finer parameterisation. A layer-stripping approach was used during inversion and modelling. Travel times of waves reflected from the top of a layer, travelling as a head-wave on top of it or refracted into the layer, were used to compute depth nodes delineating the interface at the top of the layer and velocities at top and bottom of the layer.

The initial model used for the inversion scheme was a 1-D model derived from preliminary interpretation of OBS record section 3. It consists of five layers: water layer, sedimentary layer, layer 2, layer 3 and upper mantle. Travel times of waves PbP, P2, P3, PmP and Pn were inverted. The final model (Figure 4) allows a reasonable fit for computed travel times with data leading to a RMS misfit of 65 ms for the whole data set (Figures 3 and 5 and Table 1).

The thickness of the sedimentary layer varies from 30 to 300 m. Such a thickness is rather thin for a Cretaceous oceanic crust and suggests that strong deep currents, related to the vicinity of the KP, prevented sedimentary deposits and possibly eroded the sedimentary cover.

Velocities in layer 2 vary from $5.00 \, km \, s^{-1}$ at the top of the layer at depths of 4.4 to 5.1 km, and 6.3 to $6.5 \, km \, s^{-1}$ at the bottom of the layer, yielding an average downward vertical velocity gradient of $0.44 \, s^{-1}$.

Velocities in layer 3 vary from 6.70 to $6.87 \, km \, s^{-1}$ at the top of the layer, between 6.0 and
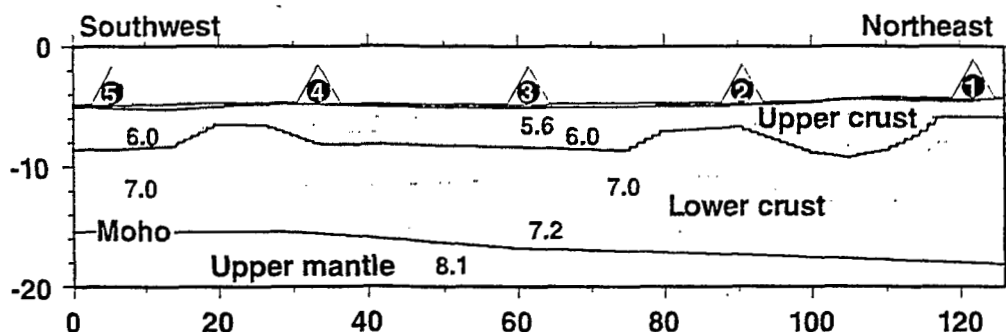
Fig. 4. Best fitting velocity model along line 7 (Enderby Basin) from 2-D inversion of travel times. Dashed lines are isovelocity contours with annotations (km s^{-1}). Plain lines delineate main crustal layers (i.e., sedimentary layer, layer 2, layer 3 and upper mantle). Location of OBSs along the profile is shown.

9.3 km deep, and 7.24 to 7.32 km s^{-1} at the bottom of the layer. The downward vertical velocity gradient is ~0.049 s^{-1} in the central part of the model.

The Moho deepens from ~15 km to ~18 km toward the KP and is associated with a thickening of the igneous crust from ~10 to ~14 km in the same direction. The thickness of layer 2 varies strongly from 1.5 to 3.7 km due to the complex topography of the top of the igneous crust and of the layer 2–layer 3 interface. The thickness of layer 3 increases from 8.3 km south-westward to 11.5 km toward the KP. The velocity at the top of upper mantle is 8.1 km s^{-1}.

2.2.2. Uncertainty analysis

In the case of a structure with strong lateral variations. uncertainties in velocities and depths are mainly a trade-off between the dip of the interface. velocity beneath the interface and the vertical velocity gradient in the overlying layer. The uncertainty in velocities in layer 2 and 3 and on the depth of the Moho can be estimated using the perturbation method described in Zelt and Smith (1992). The threshold for the RMS misfit, based on the qualitative observation of the RMS misfit curves (Fig. 5), corresponds to a 25% increase of the minimum RMS misfit. A model parameter that leads to a RMS misfit lower than this threshold provides a potential value for this parameter. The difference between the minimum and the maximum values gives the uncertainty of the model parameter.

Firstly. velocity at the top of layer 2 is kept constant at a value of 5.0 km s^{-1} and a perturbation is applied to velocities at the bottom of layer 2. Secondly. we compute the depth of the layer 2–layer 3 interface in the central part of the line (where structures are poorly affected by lateral variations allowing an reliable inversion) inverting travel times of waves P2. P3 and PmP [Fig. 5(a)].

The uncertainty in the velocity at the bottom of layer 2 is ~0.2 km s^{-1} (velocity of 6.0±0.2 km s^{-1} in the centre of the model). it corresponds to an uncertainty of ±1 km in the depth of the layer 2–layer 3 interface.

Velocity at the top of layer 3 is computed for different values of the downward vertical velocity gradient inverting travel times of wave P3 [Fig. 5(b)]. Vertical velocity gradients between 0.00 and 0.08 s^{-1} are acceptable (RMS < 0.07. N_{Tobs} > 815). The vertical velocity gradient that mini-
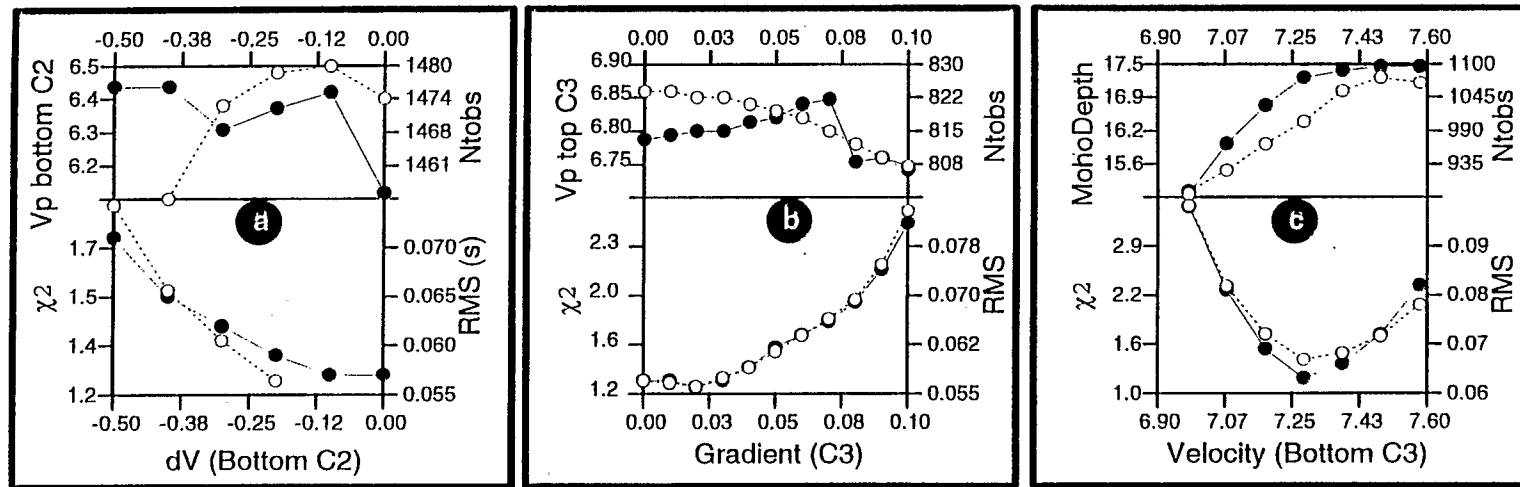
Fig. 5. Analysis of uncertainty of velocities in layer 2 and 3 and of the depth of the Moho. (a) Several parameters are plotted as a function of the perturbation applied to the bottom velocity in layer 2 (dV, km s^{-1}). Lower panel: root mean square (RMS, s) misfit between observed and computed travel times of waves P2, P3 and PmP (filled circles), χ^2 (empty circles). Upper panel: N_{Tobs} is the number of observations to which rays were successfully traced (filled circles), V_p is the velocity (km s^{-1}) at the bottom of layer 2 after the inversion (empty circles). (b) Parameters are plotted as a function of vertical velocity gradient in layer 3 (s^{-1}). Lower panel: RMS (s) misfit between observed and computed travel times of waves P3 (filled circles), χ^2 (empty circles). Upper panel: as in Fig. 5(a), V_p (km s^{-1}) at the top of layer 3 after the inversion (empty circles). (c) Parameters are plotted as a function of velocity at the bottom of layer 3 (km s^{-1}). Lower panel: RMS (s) misfit between observed and computed travel times of waves P3 and PmP (filled circles), χ^2 (empty circles). Upper panel: as in Fig. 5(a), depth of the Moho (km) computed using travel times of P3 and PmP (empty circles).

Table 1
Results of the travel time inversion along line 7

Phase	Layer	N_{Tobs}	N_z	N_{vs}	N_{vi}	RMS (s)	χ^2
PbP and P2	upper crust	514	16	1	19	0.037	0.727
P3	Lower crust	829	19	6	6	0.063	1.493
PmP and Pn	Upper mantle	553	5	1	1	0.150	3.505

Phase = phase used for inversion; PbP = reflection from top of igneous crust; P2 = refraction in upper crust; P3 = refraction in lower crust; PmP = reflection from Moho; Pn = refraction in upper mantle; Layer = layers of the model perturbed for the inversion; depth to the top of the layer and velocity at the top and at the bottom of the layer are computed; NTobs = Number of observed travel times used for the inversion; Nz = Number of depth nodes computed for the inversion; Nvs = Number of upper velocity nodes computed for the inversion; Nvi = Number of lower velocity nodes computed for the inversion; RMS = RMS misfit.

mises the RMS misfit is $0.025\,\text{s}^{-1}$. The range of gradient obtained leads to a velocity at the top of layer 3 of $6.82 \pm 0.03\,\text{km s}^{-1}$.

To estimate the uncertainty on the velocities at the base of layer 3 and on the depths of the Moho, a perturbation was first applied to the bottom velocity, the top velocity remaining constant. The Moho depth is computed using P3 and PmP travel times [Fig. 5(c)]. The best result is obtained for a velocity of $7.28\,\text{km s}^{-1}$ at the base of layer 3 with an uncertainty of $\sim 0.3\,\text{km s}^{-1}$. The Moho depth is $16 \pm 1\,\text{km}$ in the central part of the model [Fig. 5(c)].

2.2.3. Synthetic seismograms

Synthetic seismograms were computed to more accurately determine the vertical velocity gradients and to improve the velocity versus depth function. The reflectivity method (Fuchs and Müller, 1971) was used to model the crust from the OBS 3 record section as plane and horizontal layers of constant velocity. This modelling is reliable as 2-D travel time modelling validated the assumption of 1-D velocity structure close to OBS 3. Nevertheless, the two parts of the record section, at either sides of OBS 3, were modelled separately to take into account finer details in the structure (Figure 6). No anelastic attenuation was taken into account for the computation of synthetic seismograms.

Layer 2 is composed of 2 sub-layers (uc1 and uc2) separated by a 100–200 m-thick transition zone with a high velocity gradient that generates the high amplitude observed around 8.5 km. Seismic velocities range from $4.65\,\text{km s}^{-1}$ to $5.20\,\text{km s}^{-1}$ in the upper sub-layer and from 5.60 to $6.30–6.75\,\text{km s}^{-1}$ in the lower sub-layer. Velocities at the bottom of layer 2 vary significantly on either side of the OBS (6.30 and $6.75\,\text{km s}^{-1}$). They are constrained by the post-critical travel time arrival and the maximum amplitude of the wave reflected from the layer 2–layer 3 interface. This difference can be ascribed to a two-dimensional effect or variation in porosity (Operto, 1995). The velocity in layer 3 increases steadily from $7.00–7.05\,\text{km s}^{-1}$ at the top to $7.40–7.50\,\text{km s}^{-1}$ at the bottom at a depth of 15.7 km.

High amplitudes of the PmP are recorded between 40 and 45 km, a low at 50 km and a second high at 60 km (Fig. 6). We assume that the first amplitude high at 40–45 km is related to the
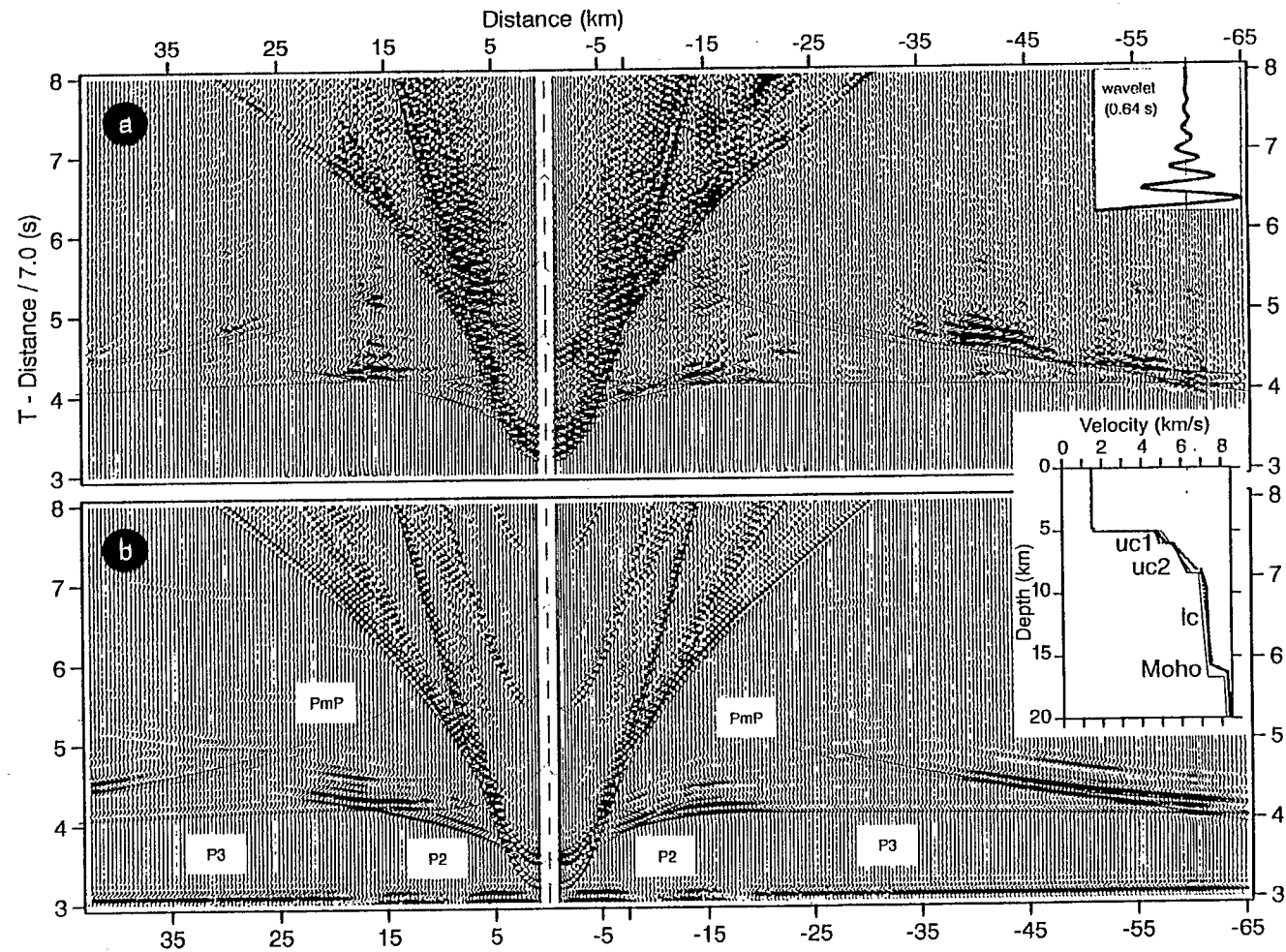
Fig. 6. (a) Upper panel: OBS 3 record section with amplitude scaled proportional to range. Computed travel times are superimposed. The inset shows the wavelet convolved with the impulsive synthetic seismograms. (b) Lower panel: reflectivity synthetic seismograms computed for OBS 3. The inset shows 1-D velocity models used for the computation of synthetic seismograms for positive offsets (plain line) and negative offsets (dashed line). The thin plain line corresponds to the velocity function beneath OBS 3 in the 2-D best fitting model Fig. 4.

critical distance whereas the second amplitude high is related to a constructive interference between the PmP and P3 waves. To account for the very low amplitude of the pre-critical PmP, the Moho located at 16.5 km depth was modelled as a 800 m-thick transition zone between the lowermost crustal velocity of 7.50 km s^{-1} and the uppermost mantle velocity of 8.3 km s^{-1}.

2.2.4. Crustal thickness and sub-divisions

Crustal velocities below the Enderby Basin are within the range of those reported for oceanic layer 2 and 3 (2.5 to 6.6 km s^{-1} and 6.6 to 7.6 km s^{-1}, respectively, White et al., 1992). The sedimentary cover is very thin and absent in places. The igneous crust thins south-westward from 13.5 km near the KP to 10.0 km. According to the classification of White et al. (1992), the crust of the Enderby Basin is slightly thicker than standard oceanic crust (7.08 ± 0.78, White et al., 1992) but is consistent with oceanic crust affected by hot mantle plume (10.3 ± 1.7 km, White et al., 1992). The thinning of the igneous crust observed away from the plateau is mainly caused by the layer 3 thinning (from 11 km to 7 km). The thickness of layer 2 is highly variable (between 1.5 and 4.9 km) but with no obvious relation to its proximity to the KP. This is in good agreement with the thickening of most oceanic crust emplaced at ridges that is dominated by thickening of layer 3 (Mutter and Mutter, 1993). The ratio between layer 3 and layer 2 thicknesses calculated in the middle of seismic line 7 is 3.8. It is higher than the value of 2.4 obtained for standard oceanic crust but it is close to the value of 3.9 calculated for the crust beneath Iceland (Mutter and Mutter, 1993). Velocity at the base of the crust, beneath the Enderby Basin reaches 7.4–7.5 km s^{-1} but there is no evidence of a high-velocity body, located between the crust and the upper mantle, as observed beneath some intraplate islands (e.g., Hawaii, Watts and ten Brink, 1989; Marquesas Islands, Caress et al., 1995). Seismic velocities increase gently from ~7.00 to ~7.50 km s^{-1} in layer 3. The average velocity in this layer (~7.25 km s^{-1}) suggests an increased contribution of ultramafic rocks, possibly related to an increase in the potential temperature during melting (White and McKenzie, 1989; Mutter and Mutter, 1993). A 100°C increase of the potential temperature is necessary to create a ~13 km thick oceanic crust (White and McKenzie, 1989).

3. The northern Kerguelen plateau

Two wide-angle seismic profiles were shot on the northern KP between Kerguelen and Heard islands (Fig. 1). Travel time inversion (Charvis et al., 1995) shows a 19 to 21 km thick igneous crust composed of 3 layers (Figure 7). The upper layer is 1.2–2.3 km-thick, velocities ranging from 3.80 to 4.90 km s^{-1}. It could be composed of either low-density lava flows or volcanic material interlayered with sediments (Munschy and Schlich, 1987; Charvis et al., 1995). The second layer is 2.3–3.3 km thick, velocities ranging from 4.70 km s^{-1} to 6.70 km s^{-1} downward. In the lower crust, velocities increase from 6.60 km s^{-1} at ~8.0 km depth (near the top of the layer) to 7.40 km s^{-1} at the base of the crust with no internal discontinuity. Moreover, poor PmP and the lack of Pn (except on OBS 3 and OBS 5 record sections, Figures 7 and 8 of Charvis et al., 1995) suggest that the Moho is a gradual transition zone and that the velocity gradient is low in the upper mantle (Operto, 1995). No attempt has been made to model the crust–mantle transition using reflectivity synthetic seismograms, the lateral variations of the amplitude of PmP
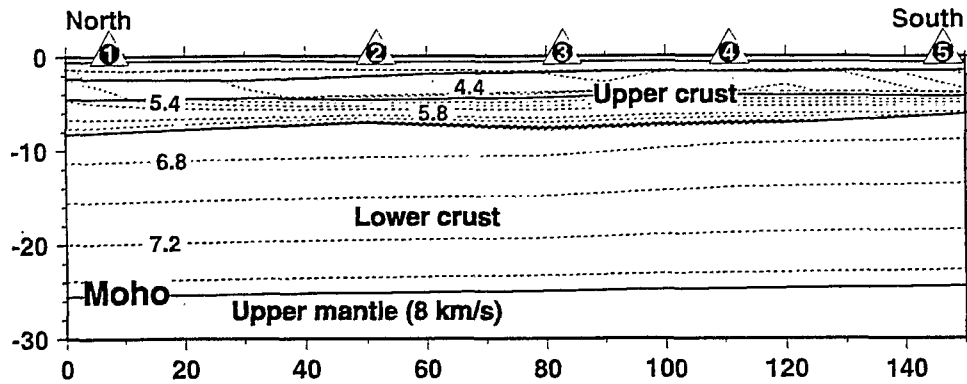
Fig. 7. Best fitting velocity model across line 1 (northern Kerguelen Plateau) from 2-D inversion of travel times (after Charvis et al., 1995). Dashed lines are isovelocity contours with annotations (km s^{-1}). Plain lines delineate main crustal layers (i.e., sedimentary layer, layer 2, layer 3 and upper mantle). Location of OBSs along the profile is shown.

wave from one OBS to another along lines 1 and 2 being too strong (Figures 7 and 8 of Charvis et al., 1995).

3.1. Synthetic seismograms

Reflectivity synthetic seismograms were computed only for OBSs 1 and 2 of line 1 and OBS 4 of line 2 assuming low lateral variations along these lines. The 0.8–1.0 km-thick sedimentary cover is split into two layers with velocities ranging from 1.60 km s^{-1} at the top of the upper layer to 2.5–3.0 km s^{-1} at the bottom of the lower layer. The upper crust consists of three units. The uppermost unit (uc1) is 0.4–0.9 km thick, with velocities ranging from 3.00–4.60 km s^{-1} at the top to 3.06–4.85 km s^{-1} at the bottom, with a vertical velocity gradient of 0.14–0.37 s^{-1}. The low-velocity layer (lvz), located below uc1, is outlined by a shadow zone on seismic record sections (Figures 7–10). Velocities in this layer are not well constrained from our data set mainly because reflected waves from the top of layer uc2 (Pruc2) interfere with those refracted in layer 2 (Puc2), precluding an accurate amplitude modelling. Nevertheless, velocities range from 2.50 to 4.40 km s^{-1} and thicknesses range between 0.5 to 1.6 km. The lowermost unit of the upper crust (uc2) is 2.6–4.9 km thick, with velocities increasing from 4.00–5.00 km s^{-1} at the top of the layer to 6.48–6.58 km s^{-1} at the bottom, with a vertical gradient of 0.41–0.58 s^{-1}. To complement a qualitative comparison between computed and observed amplitudes and waveforms, we compare the maximum amplitude distance curves with respect to offset for the synthetic and observed sections (Fig. 10). The amplitude decay of wave Plc (refracted in the lower crust) around 30 km of distance on OBS record section 4 of line 2 (Fig. 9) was modelled by a decrease of the vertical velocity gradient in the lower crust from 0.1 s^{-1} in the first upper kilometre to 0.03 s^{-1} below.

3.2. Crustal subdivisions

Three major improvements to the velocity model computed from travel time inversion of Charvis et al. (1995) have been implemented: (1) the modelling of the low-velocity layer (lvz) sandwiched between layers uc1 and uc2 (Figures 8–10); (2) the larger vertical velocity gradient
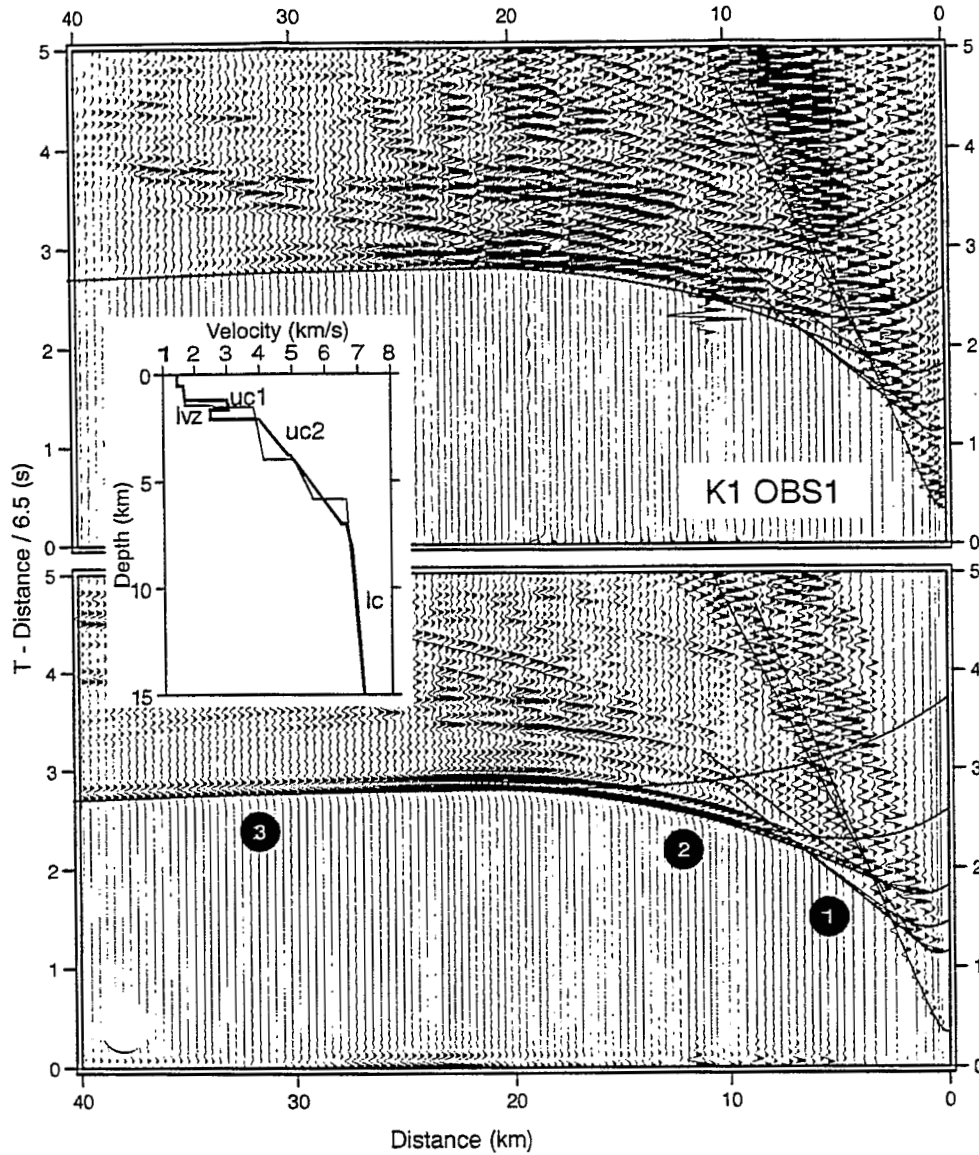
Fig. 8. Upper panel: OBS 1 (line 1, northern Kerguelen Plateau) record section with amplitude scaled proportional to range. Lower panel: synthetic seismograms computed for OBS 1 (velocity function shown in inset). Labels 1, 2, 3 refer to phases Puc1, Puc2 and Plc, respectively. Inset: Thick line: 1-D velocity models inferred from synthetic seismogram modelling for OBS 1 (line 1); thin line: velocity function beneath OBS 1 from the 2-D model computed from travel times inversion (Charvis et al., 1995).

in layer uc2 to account for the important curvature of arrival Puc2, the strong amplitude and the smooth connection with arrival Plc (refracted from layer lc) (there is no break between the slope of arrival Puc2 and the slope of arrival Plc); (3) the greater depth of the uc2–lc interface to fit the amplitude at the Puc2–Plc cusp and the travel time of Plc. This increase is mainly related to the increase of the average velocity in layer uc2.
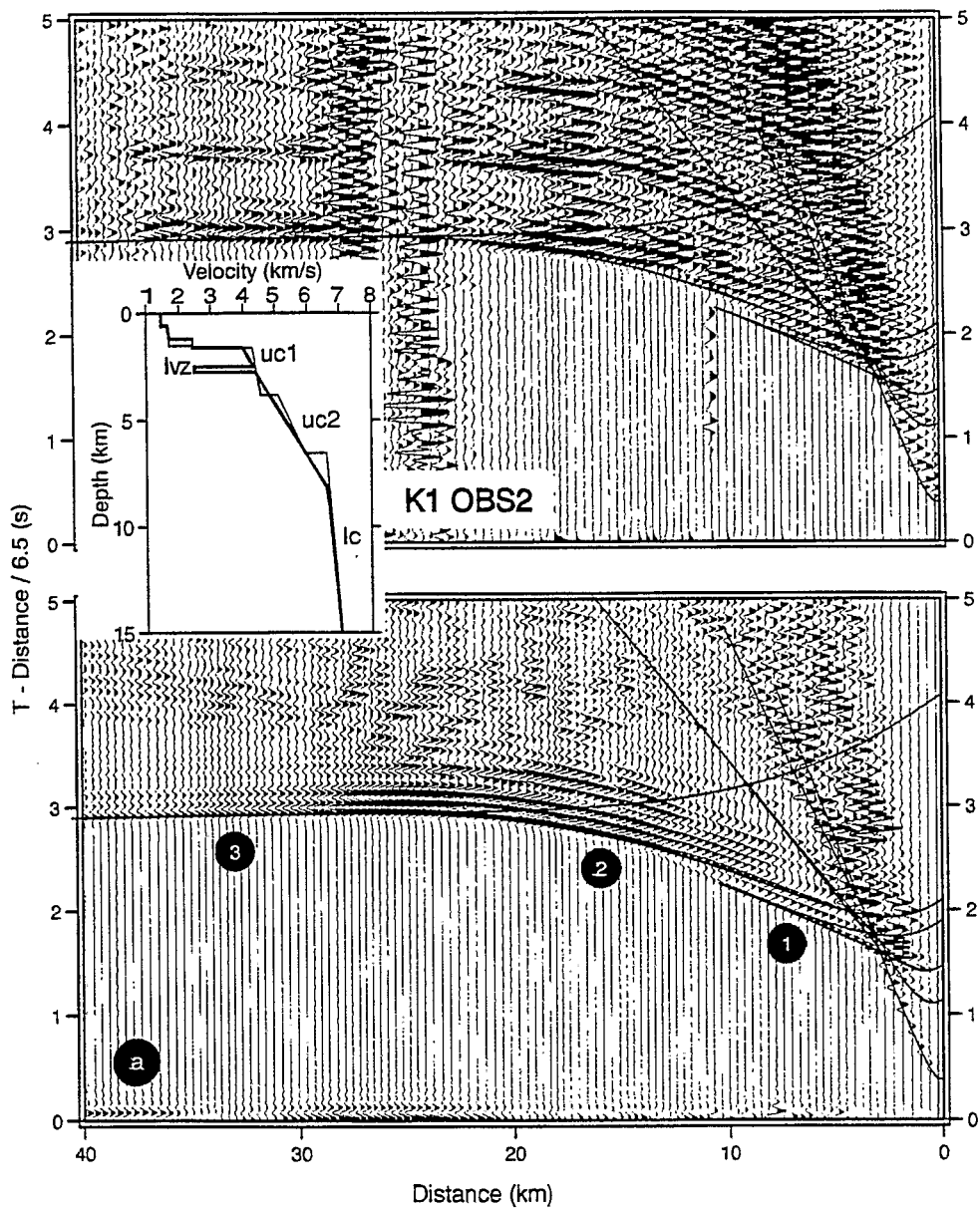
Fig. 9. Caption opposite.

The nature of layers uc1 and lvz is still a matter of debate (Munschy and Schlich, 1987; Charvis et al., 1995) as observed seismic velocities are highly variable and can be either related to consolidated sediments or altered volcanic rocks. Only layer uc2 can be interpreted as a basaltic layer from seismic velocities. Nevertheless, the presence of large lateral variations observed in both layers uc1 and lvz are more consistent with lava flows, possibly partly altered, inter-layered
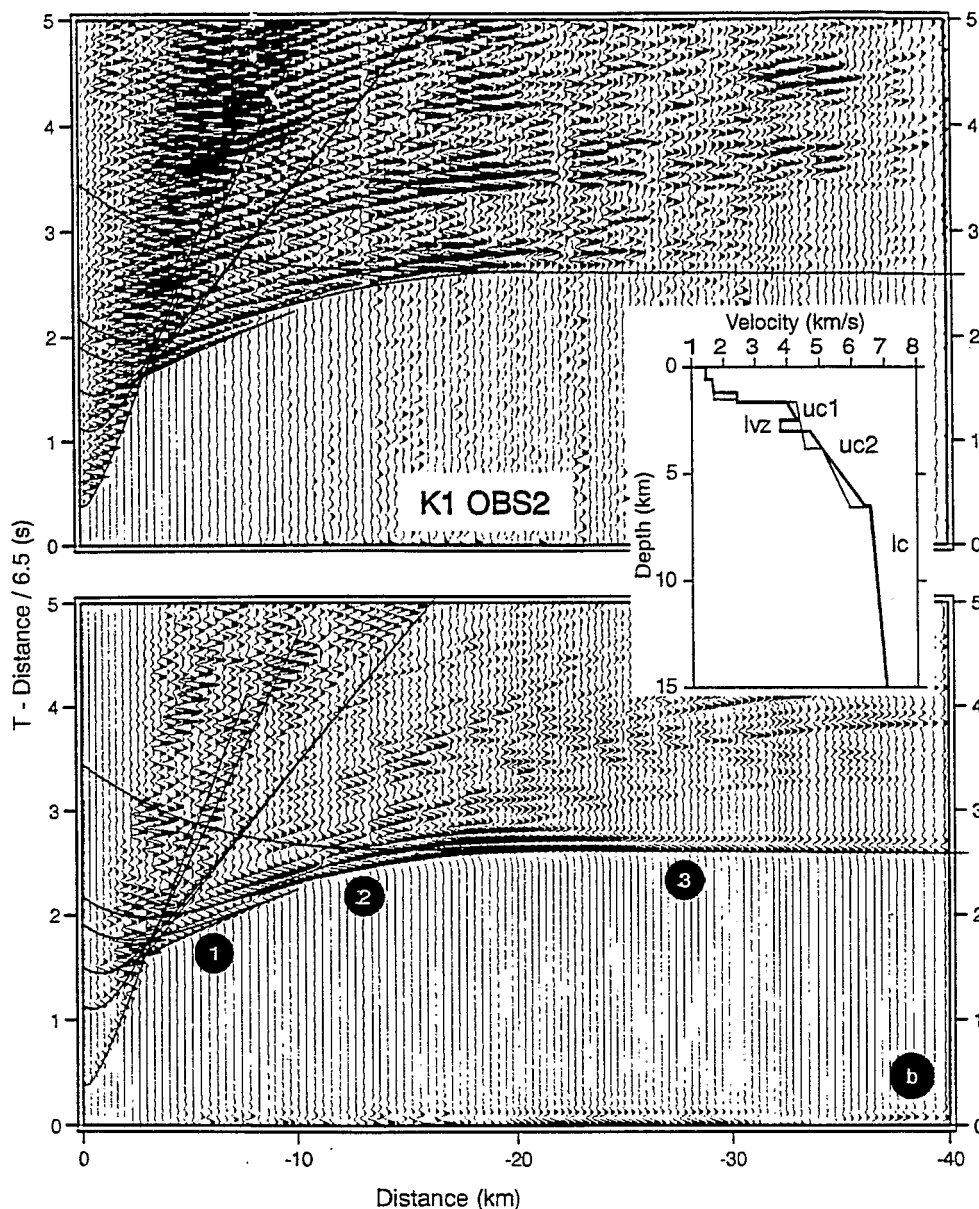
Fig. 9. Same as Fig. 8 for OBS 2 line 1 positive distances (a) and negative distances (b).

with volcano–sedimentary material than with a purely sedimentary pile where seismic velocity is mostly governed by compaction. Velocities and vertical velocity gradient in layer uc2 are consistent with those observed in basaltic layer 2 of the oceanic crust. Furthermore, the lack of first order velocity discontinuity between layer uc2 and layer lc is similar to the typical transition observed between oceanic layers 2 and 3.
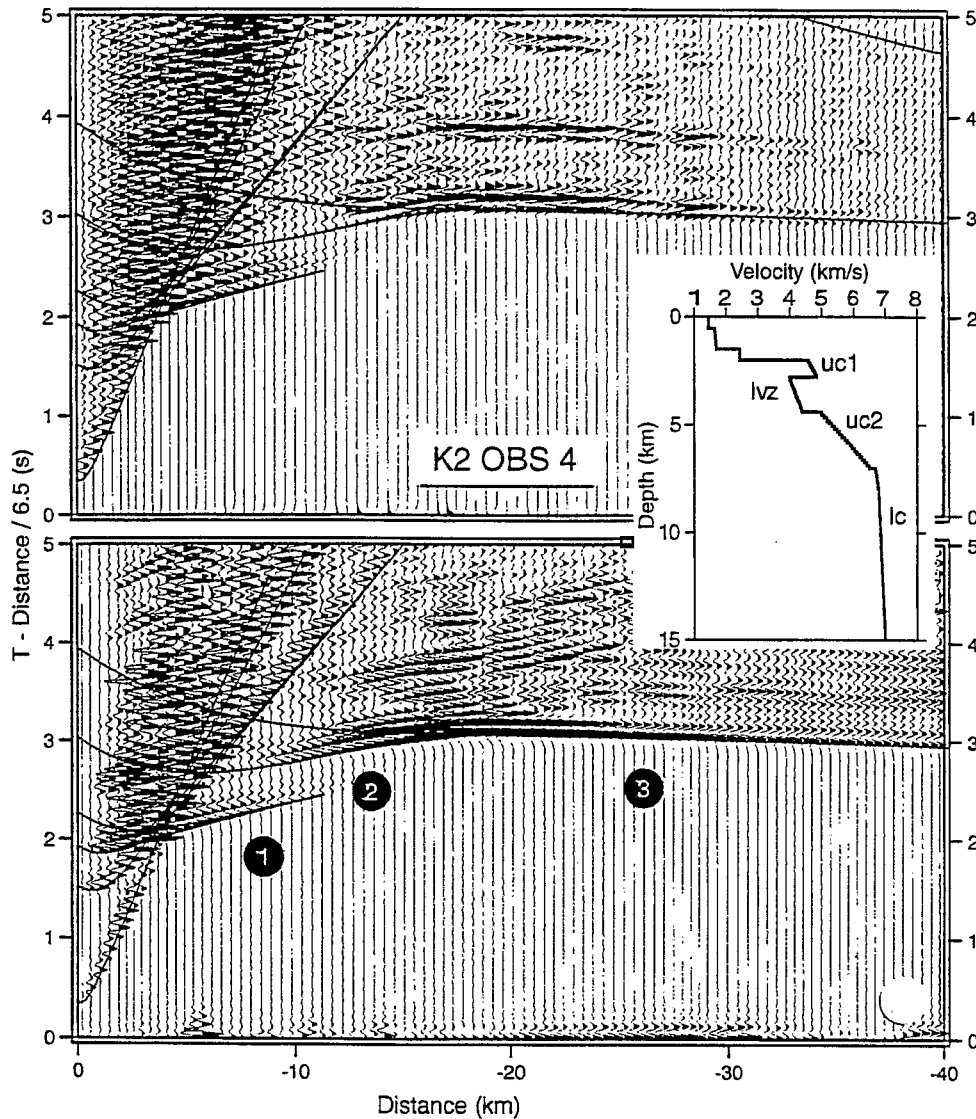
Fig. 10. Same as Fig. 8 for OBS 4 line 2.

4. Discussion and conclusions

For their kinematic reconstructions, Royer and Sandwell (1989) assumed that the formation of the Enderby Basin was synchronous with both the formation of the Perth and Cuvier Basins (anomalies M0 to M10, west of Australia) and the emplacement of the southern KP, although no magnetic anomaly in the Enderby Basin support this interpretation. The depth of the Enderby Basin at line 7 is ~5 km whereas the predicted depth for a 80–120 Ma-old oceanic basin is 5.6–6.0 km (Parsons and Sclater, 1977) leading to a depth anomaly of ~0.8 km. The crust of the

Enderby Basin is 10 to 13 km-thick and thins gently away from the plateau, indicating that it was probably affected by the Kerguelen mantle plume. Velocities in layer 3 are 6.90–7.00 km s^{-1} at the top (at ~8 km depth) and 7.40–7.50 km s^{-1} at the base of the crust (at ~16 km depth). These higher velocities than those found in normal oceanic crust are very close to those determined in the North Atlantic oceanic basins around Iceland (e.g., Ritzert and Jacoby, 1985; Fowler et al., 1989) and comply with an olivine-rich gabbros composition of the crust. This feature suggests that the Enderby Basin oceanic crust formed at a spreading centre that traversed the region of unusually hot mantle surrounding the Kerguelen hotspot.

The total thickness of the sedimentary cover of the northern KP ranges from 1.6 to 2.1 km (this paper and Charvis et al., 1995). This is in good agreement with thicknesses previously determined from sonobuoy measurements (Houtz et al., 1977; Munschy and Schlich, 1987). A major discordance, related to the rifting between the northern KP and Broken Ridge at 43 Ma splits the sedimentary cover into two sequences (Houtz et al., 1977; Wicquart and Fröhlich, 1986; Munschy and Schlich, 1987). Samples from the ~1200 m-thick lower sequence were dated, using micro-fossils, as old as Santonian, 85 Ma (Wicquart and Fröhlich, 1986). Nevertheless, Santonian samples are not the oldest deposits and Wicquart and Fröhlich (1986), using an extrapolation of the sedimentation rate for the lower sequence (20 m/My), inferred a possible age of 100 to 120 Ma for the oldest deposits near the eastern flank of the KP. This age is consistent with other biostratigraphic dating and with ages obtained from radiometric dating of basaltic samples from the basement of the southern KP (Leclaire et al., 1987; Whitechurch et al., 1992). This strongly suggests that the whole upper crust, including layers uc1, lvz and uc2, was emplaced before 100–120 Ma simultaneously with the Cretaceous KP and is not related to a more recent period.

The complex structure of the upper crust beneath the northern KP suggests several successive phases of volcanism leading to a complex accumulation of volcanic flows and possibly inter-layered sediments. Layers uc2 and lc, separated by a second order discontinuity, are akin to thickened oceanic crust and probably resulted from a primary magmatic event. Layer lvz could be related to a phase of sedimentation and alteration of the basaltic basement devoid of major volcanic activity whereas layer uc1 was built during a second phase of volcanic activity. The highly variable but generally low velocities observed in layer uc1 suggest that this layer consists either of alternate sedimentary and volcanic material or altered lava flows. Low velocities observed in the upper crust down to 2.4 km below the top of basement (Figures 8–10) suggest that it could result from several phases of volcanic activity separated by periods of alteration and sedimentation rather than a single major volcanic phase continuously producing the whole layer. An alteration of a homogeneous volcanic pile would have generated a high vertical velocity gradient as it is usually observed in oceanic layer 2 (White et al., 1992).

A second volcanic phase, 20 to 40 Ma after the first one, is often observed in large volcanic provinces (e.g., 120–122 Ma and 88–90 Ma for the Ontong Java Plateau, 110–114 Ma and 85 Ma for the southern KP, Whitechurch et al., 1992; Bercovici and Mahoney, 1994; Pringle et al., 1994). Furthermore, the northern KP was affected by Tertiary volcanic activity mainly noticed on the Kerguelen Archipelago and in Heard and McDonald islands (Giret, 1983) and related to the recent activity of the Kerguelen Hotspot (Royer and Coffin, 1992; Müller et al., 1993). Several gravimetric highs aligned between the Kerguelen and Heard Island, west of the seismic lines (Fig. 1) suggest that the tertiary volcanic activity also affected the submarine plateau. We believe that

the northern KP results from a long-term evolution like today's Iceland with successive phases of volcanic activity starting 100–120 M.y. ago until the quaternary volcanism of the Kerguelen and Heard islands, rather than a transient volcanic event as suggested for some large igneous provinces (Coffin and Eldholm, 1994).

The Cretaceous Kerguelen Volcanic province, including the KP and part of the surrounding oceanic basins (i.e., the Enderby Basin), is similar in size to the North Atlantic Volcanic Province and may be the result of a similar process. Comparison between the Enderby Basin and the northern KP velocity structures also shows that velocities at a given depth are higher below the Enderby Basin than below the northern KP but the crust is thinner below the Enderby Basin. The indisputable oceanic origin of the northern KP suggests that it was formed in cooler conditions, maybe during a latter phase of activity of the Kerguelen hotspot. The velocity structure of the northern KP matches quite well the age-progressive plume model of Farnetani and Richards (1994) and is very close to that of Iceland.

Velocities in layer 3 of the Enderby Basin are significantly higher than those of the lower crust of Raggatt Basin in the southern KP, although the crust is thinner below the Enderby Basin. This disagrees with the conclusions of White and McKenzie (1989) and Mutter and Mutter (1993) who postulated a positive correlation between crustal thickness and velocities in layer 3. This precludes an oceanic origin for the Raggatt Basin that was interpreted as a continental fragment overlain by basaltic flows (Operto, 1995; Operto and Charvis, 1996). Comparison between velocity structures of the northern KP and the Raggatt Basin also corroborates this interpretation. The velocity structure in the northern KP is characterised by very smooth transitions between layers uc2 and lc (Figures 8–11) and between layers lc and the upper mantle, leading to a seismically transparent structure (Charvis et al., 1995). On the contrary, the first-order discontinuity between upper crust and lower crust, the layered lower crust and the highly reflective Moho observed below the Raggatt Basin are inconsistent with an oceanic origin (Operto, 1995; Operto and Charvis, 1996). Thus, the Raggatt Basin is interpreted as a continental fragment, analogous to the Rockall Plateau edging the eastern margin of the North Atlantic Volcanic Province (Operto, 1995; Operto and Charvis, 1995; Operto and Charvis, 1996). Magmatism affecting the upper structure of Raggatt Basin may be a result of the initial activity of the Kerguelen mantle plume.

We propose that the KP is the result of a long-term discontinuous evolution with successive phases. A preliminary phase of continental rifting emplaced the southern KP under the influence of the Kerguelen plume head. Part of the southern KP constitutes a fragment of the Australian–Antarctic volcanic continental margin. The Enderby Basin could have formed away from the plume head but its structure is clearly affected by this plume. The high velocities in the crust of the Enderby Basin may result from hot mantle material generated by the first activity of the plume. The emplacement of the northern Kerguelen oceanic Plateau is related to the subsequent activity of the plume, with a cooler mantle leading to lower velocities in the crust, in a setting similar to Iceland today, following the age-progressive plume model of Farnetani and Richards (1994).

This scheme for the formation of the KP requires further kinematic reconstructions to be validated as the current reconstructions preclude continental fragments between India and the Australian–Antarctic plate (Royer and Sandwell, 1989; Royer and Coffin, 1992). Nevertheless, we have shown that comparison between velocity structures of the three domains investigated in
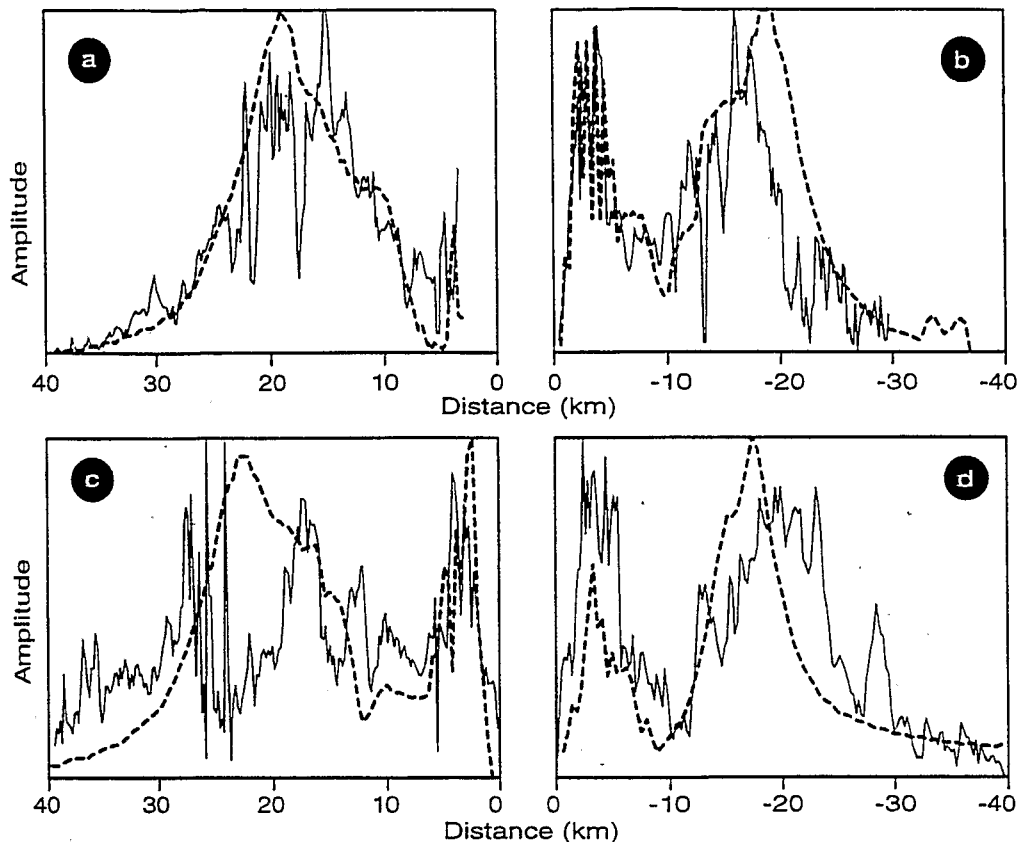
Fig. 11. Maximum amplitude versus offset curves for OBSs 1 (a) and 2 (b, c) of line 1 and for OBS 4 for line 2 (d). Plain line is the amplitude measured in a 0.2 s time-window on the data for phases Pw (water wave), Puc1, Puc2 and Plc. The dashed line is the amplitude from computed synthetic seismograms. The first amplitude high is associated with the reflection from top of layer uc1 at critical distance followed by an amplitude decreasing associated with the refraction in layer uc1. The second amplitude high is related to the wave Puc2 followed by amplitude decreasing related to refraction in the lower crust. All these features are properly modelled. On panel c, amplitude decreasing at ∼25 km of distance is due to noisy traces.

this study (northern and southern KP and the Enderby Basin) rules out a single process for the formation of the entire plateau.

Geoffroy Lamarche and Maurice Recq for their help in editing the manuscript and J. Ansorge and J. Gallart for reviewing the manuscript.

UMR 6526 contribution 129.

References

Bercovici, D., Mahoney, J., 1994. Double flood basalts and plume head separation at the 660-kilometer discontinuity. Science 266, 1367–1369.

Caress, D.W., McNutt, M.K., Detrick, R.S., Mutter, J.C., 1995. Seismic imaging of hotspot-related crustal underplating beneath the Marquesas Islands. Nature 373, 600–603.

Charvis, P., Recq, M., Operto, S., Bréfort, D., 1995. Deep structure of the northern Kerguelen-Plateau and hotspot-related activity. Geophys. J. Int. 122, 899–924.

Coffin, M.F., Davies, H.L., Haxby, W.F., 1986. Structure of the Kerguelen Plateau province from seasat altimetry and seismic reflection data. Nature 324, 134–136.

Coffin, M.F., Eldholm, O., 1994. Large igneous provinces: crustal structure. dimensions, and external consequences. Rev. Geophys. 32, 1–36.

Farnetani, C., Richards, M.A., 1994. Numerical investigations of the mantle plume initiation model for flood basalt events. J. Geophys. Res. 99, 13813–13833.

Fowler, S.R., White, R.S., Spence, G.D., Westbrook, G.K., 1989. The Hatton Bank continental margin—II. Deep structure from two-ship expanding spread seismic profiles. Geophys. J. 96, 295–309.

Fuchs, K., Müller, G., 1971. Computation of synthetic seismograms with the reflectivity method and comparison with observations. Geophys. J. R. Astron. Soc. 23, 417–433.

Giret, A., 1983. Le Plutonisme Intraplaque: Exemple de l'Archipel Kerguelen (TAAF). Comité National Français de la Recherche Antarctique, Paris, pp. 290.

Houtz, R.E., Hayes, D.E., Markl, R.G., 1977. Kerguelen Plateau bathymetry. sediment distribution and crustal structure. Mar. Geol. 25, 95–130.

Leclaire, L., Bassias, Y., Denis-Clocchiatti, M., Davies, H., Gautier, I., Gensous, B., Giannesini, P.-J., Patriat, P., Ségoufin, J., Tesson, M., Wannesson, J., 1987. Lower cretaceous basalt and sediments from the Kerguelen Plateau. Geo. Mar. Lett. 7, 169–176.

Müller, R.D., Royer, J.-Y., Lawver, L.A., 1993. Revised plate motions relative to the hotspots from combined Atlantic and Indian Ocean hotspot tracks. Geology 21, 275–278.

Munschy, M., Dyment, J., Boulanger, M.O., Boulanger, D., Tissot, J.D., Schlich, R., Rotstein, Y., Coffin, M.F., 1992. Breakup and seafloor spreading between the Kerguelen Plateau–Labuan Basin and the Broken Ridge–Diamantina Zone. In: Wise, S.W., Schlich, R. et al., (Eds.), Proceedings of the Ocean Drill. Program. Sci. Results. Ocean Drilling Program. College Station TX, 120, pp. 931–944.

Munschy, M., Schlich, R., 1987. Structure and evolution of the Kerguelen–Heard plateau (Indian Ocean) deduced from seismic stratigraphy studies. Mar. Geol. 76, 131–152.

Mutter, C.Z., Mutter, J.C., 1993. Variations in thickness of layer 3 dominate oceanic crustal structure. Earth Planet. Sci. Lett. 117, 295–317.

Nakamura, Y., Donoho, P.L., Roper, P.H., McPherson, P., 1987. Large-offset seismic surveying ocean-bottom seismographs and air guns: Instrumentation and field technique. Geophysics 52, 1601–1611.

National Geophysical Data Center, 1988. ETOPO-5 bathymetry topography data. Publ. 88-MGG-02, Natl. Oceanic and Atmos. Admin., Boulder, Colorado.

Operto, S., 1995. Structure et origine du plateau de Kerguelen (océan Indien austral): Implications géodynamiques. Modélisation de données sismiques grand-angle marines. Thèse d'université, Éditions ORSTOM, TDM No. 143, Université Pierre et Marie Curie, 292 pages.

Operto, S., Charvis, P., 1995. Kerguelen Plateau: a volcanic passive margin fragment?. Geology 23, 137–140.

Operto, S., Charvis, P., 1996. Deep structure of the southern Kerguelen Plateau (southern Indian Ocean) from wide-angle seismic data. J. Geophys. Res. 101, 25077–25103.

Parsons, B., Sclater, J.G., 1977. An analysis of variation of ocean floor bathymetry and heat flow with age. J. Geophys. Res. 82, 803–827.

Pringle, M.S., Storey, M., Wijbrans, J., 1994. ^{40}Ar/^{39}Ar geochronology of mid-Cretaceous Indian Ocean basalts: Constraints on the origin of large flood basalt provinces. In: Fall Meet. Suppl., San Francisco, Eos Trans. AGU 75, p. 728.

Ritzert, M., Jacoby, W.R., 1985. On the lithospheric seismic structure of Reykjanes ridge at 62.5°N. J. Geophys. Res. 90, 10117–10128.

Royer, J.-Y., Coffin, M.F., 1992. Jurassic to Eocene plate tectonic reconstructions in the Kerguelen plateau region. In: Wise, S.W., Schlich R. et al. (Eds.), Proceedings of the Ocean Drill. Program, Sci. Results, Vol. 120. Ocean Drilling Program, College Station TX, pp. 917–928

Royer, J.Y., Sandwell, D.T., 1989. Evolution of the eastern Indian Ocean since the Late Cretaceous: Constraints from Geosat altimetry. J. Geophys. Res. 94, 13755–13782.

Sandwell, D.T., Smith, W.H.F., 1994. ERS-1 geodetic mission reveals detailed tectonic structures. Fall Meet, Suppl., San Francisco, Eos Trans. AGU 155, p. 728.

Schlich, R., Coffin, M.F., Munschy, M., Stagg, H.M., Li, Z.G., Revill, K., 1987. Bathymetric chart of the Kerguelen Plateau. Joint publication, Bur. of Miner. Resour., Canberra, Australia and Inst. de Phys. du Globe, Strasbourg, France.

Schlich, R., Wise, S.W.J. et al., 1989. In: Kerguelen Plateau, Proceedings of the Oceaan Drilling Program, Initial Reports, Vol. 120. Ocean Drill. Program. College Station Texas.

Watts, A.B., ten Brink, U.S., 1989. Crustal structure, flexure, and subsidence of the Hawaiian Islands. J. Geophys. Res. 94, 10473–10500.

White, R., McKenzie, D., 1989. Magmatism at rift zones: The generation of volcanic continental margins and flood basalts. J. Geophys. Res. 94, 7685–7729.

White, R.S., McKenzie, D., O'Nions, R.K., 1992. Oceanic crustal thickness from seismic measurements and rare earth element inversions. J. Geophys. Res. 97, 19683–19715.

Whitechurch, H., Montigny, R., Sevigny, J., Storey, M., Salters, V.J.M., 1992. K–Ar and ^{40}Ar/^{39}Ar ages of Central Kerguelen Plateau basalts. In: (Wise, S.W., Schlich, R. et al., Eds.), Proceedings of the Ocean Drill. Program, Sci. Results, Vol. 120. Ocean Drilling Program, College Station TX, pp. 71–77.

Wicquart, E., Fröhlich, F., 1986. La sédimentation sur le plateau de Kerguelen–Heard. Relations avec l'évolution de l'océan Indien au Cénozoïque. Bulletin de la Société Géologique de France 8, 569–574.

Zelt. C.A., Smith, R.B., 1992. Seismic traveltime inversion for 2-D crustal velocity structure. Geophys. J. Int. 108, 16–341.